Applied Catalysis B: Environmental 90 (2009) 18–28

Contents lists available at ScienceDirect

Applied Catalysis B: Environmental

journal homepage: www.elsevier.com/locate/apcatb

Kinetic modeling of selective catalytic reduction of NO_x with octane over $Ag–Al_2O_3$

Derek Creaser [a,*], Hannes Kannisto [b], Jonas Sjöblom [a], Hanna Härelind Ingelsten [b]

[a] Chemical Reaction Engineering, Department of Chemical and Biological Engineering, Chalmers University of Technology, 412 96 Göteborg, Sweden
[b] Competence Centre for Catalysis, Department of Chemical and Biological Engineering, Chalmers University of Technology, 412 96 Göteborg, Sweden

ARTICLE INFO

Article history:
Received 10 November 2008
Received in revised form 30 January 2009
Accepted 9 February 2009
Available online 20 February 2009

Keywords:
NO_x reduction
$Ag–Al_2O_3$
SCR
n-Octane
Kinetic modeling
Hydrogen effect

ABSTRACT

A kinetic model for the selective catalytic reduction of NO_x with octane over a $Ag–Al_2O_3$ catalyst was developed. Analysis of experimental data indicated that feed concentrations of NO and hydrogen had significant effects on the NO_x conversion, indicating that nitrates poisoned the catalytic sites and hydrogen's role was to reduce nitrate species. As a result nitrate poisoning was a key component of the kinetic model. Also in the model, gas phase n-octane reacted with surface oxygen to form surface hydrocarbon intermediate species that could either reduce surface NO_2 species to nitrogen or be fully oxidized. An additional site was included in the model on which various oxidation reactions occurred when the NO_x reduction site was fully poisoned by nitrate species. The model also accounted for experimentally observed large temperature increases due to hydrogen oxidation, during hydrogen feed. The model was constructed from transient experimental data, both with and without hydrogen feed and from a range of reactant concentrations and temperatures.

1. Introduction

NO_x emissions in exhaust gases represent an environmental problem, as the NO_x causes formation of acid rain, ground level ozone and also, in some regions, contributes to eutrophication of ground and water. As legislative levels have become more and more stringent, aftertreatment is required to reduce these emissions. The three-way catalyst has been used since the 1970s for engines operating at stoichiometric conditions, effectively reducing HC, CO and NO_x emissions. Modern engines, i.e. diesel and lean-burn engines operate at oxygen excess, increasing the fuel economy, although severely decreasing the TWC's capability of reducing NO_x. One possible solution is provided by the hydrocarbon-assisted selective catalytic reduction of NO_x (HC-SCR), where silver alumina has been shown to be an efficient catalyst in both laboratory environments [1–4] and bench tests [4]. The drawback of the silver alumina system has been the poor NO_x reduction activity at low temperatures. However, addition of small amounts of hydrogen to the SCR reaction has been shown to dramatically broaden the operating window towards low temperatures, for the silver alumina catalyst [5–7].

In recent years, several studies of the H_2-assisted HC-SCR reaction over silver alumina have been reported [5–18], however the mechanism for the HC-SCR reaction, and most certainly the so-called hydrogen effect, is still under debate. Several reasons for the hydrogen effect have been proposed: indirect reasons as structural changes of the silver due to hydrogen [5,7,13,16,18], but also direct mechanistic causes [6,8–12,15,17,19] as, e.g. transformation of cyanide to isocyanate [6,12], or removal of nitrates poisoning the catalyst surface [6,8–10,15,19].

Kinetic models can provide a tool for understanding the HC-SCR reaction mechanism and they are useful for the implementation of a catalyst in an exhaust aftertreatment system. Reports concerning kinetic models for HC-SCR over silver alumina catalysts are sparse. Backman et al. [9] reported in 2006 a kinetic model for reduction of NO with n-octane in presence of hydrogen over silver alumina, however for isothermal and steady state conditions. This work presents a global kinetic model for the selective catalytic reduction of NO_x with n-octane over a $Ag–Al_2O_3$ catalyst. The model is based on the removal of nitrates, poisoning the catalytic surface, by hydrogen. It is constructed from transient experimental data both with and without hydrogen feed and from a range of reactant feed concentrations and temperatures.

2. Experimental methods

2.1. Catalyst preparation

The silver–alumina sample (BET: 196.8 $m^2\,g^{-1}$) was prepared according to a single step sol–gel method [20,21]. Aluminium isopropoxide (98+%; Aldrich) and a small quantity of 65% HNO_3 (Fluka) in the ratio of 0.195 mol HNO_3/mol AIP, were mixed in water (milli-Q; 10 ml water/g AIP) to form an aluminium hydroxide sol. Silver nitrate (>99.5%; VWR), corresponding to the

* Corresponding author. Tel.: +46 31 7723023.
E-mail address: creaser@chalmers.se (D. Creaser).

0926-3373/$ – see front matter © 2009 Elsevier B.V. All rights reserved.
doi:10.1016/j.apcatb.2009.02.005

Nomenclature

y	gas phase mole fraction
F_{tot}	total molar flow rate (mol s^{-1})
c_{tot}	total gas concentration (mol m^{-3})
c_{Pgas}	average heat capacity of the gas mixture (J mol^{-1} K^{-1})
k_c	mass transport coefficient (m s^{-1})
$k_{m,i}$	rate constant at 300 °C for reaction i (m^3 s^{-1} mol^{-1}) or (s^{-1})
E_{Ai}	activation energy for reaction i (kJ mol^{-1})
h	heat transport coefficient (J m^{-2} s^{-1} K^{-1})
ΔH_R	enthalpy of reaction (J mol^{-1})
a	mass or heat transport area in each tank (m^2)
m_{tank}	washcoat mass in each tank (kg)
m_{mono}	monolith and washcoat mass in each tank (kg)
m_p	quartz glass tube mass (kg)
N	catalyst site density (mol kg^{-1})
n_{rxn}	number of reactions
n_{tank}	number of tanks in series
c_{Pmono}	monolith and washcoat heat capacity (J kg^{-1} K^{-1})
c_{Pp}	quartz glass tube heat capacity (J kg^{-1} K^{-1})
r	reaction rate (s^{-1})
T	temperature (K)
t	time (s)
UA	heat transport coefficient between monolith and quartz glass tube (J s^{-1} K^{-1})
θ	adsorbed species surface coverage
χ	stoichiometric coefficient for adsorbed species
υ	stoichiometric coefficient for gas phase species

Subscripts

b	bulk gas
f	feed to tank
s	catalyst washcoat surface
p	quartz tube

nominal silver loading of 5 wt.%, was dissolved in water (milli-Q) and added to the sol, which was subsequently stirred for 12 h. The solvent was thereafter removed under reduced pressure at 50 °C to form a gel. The gel was dried in air at 100 °C and crushed to a fine powder, followed by calcination in air at 600 °C for 6 h. The sample was further characterized in terms of XRD, XPS and TEM, as reported in [21].

2.2. Coating of monolith substrates

A cordierite monolith (400 CPSI, 188 parallel channels with 1.1 mm channel dimension) was cut from a 20 mm block and calcined in air at 600 °C for 3 h. The silver–alumina powder was mixed with boehmite (Disperal Sol P2; Condea) in a weight ratio of 4:1 and then added to water (milli-Q) under vigorous stirring, forming a slurry containing 20% dry material. The monolith was coated by immersion in the slurry. Excess slurry was removed by gently blowing air through the channels. The coated monolith was then dried in a 90 °C air stream for approximately 10 min and subsequently calcined in hot air (~600 °C) for 1 min. The procedure was repeated until in total 0.85 g of dry material was deposited on the monolith, followed by calcination in air for 3 h at 600 °C. This final washcoat loading corresponded to 20 wt.% with an estimated average washcoat thickness of 87 μm.

2.3. Reactor experiments

The flow reactor system used for evaluation of the catalytic performance of the catalyst has been described in detail previously [22,23]. The reactor consisted of a horizontal quartz tube heated by a heating coil, where the temperature was measured by two thermocouples (type K), 15 mm before the sample and inside the monolith sample (just before the rear end), respectively. The inlet gas composition was controlled by an Environics 2000 gas mixer and the temperature before the monolith was controlled by a Eurotherm temperature controller. Argon was used as carrier gas. The total flow was 3500 ml/min, corresponding to GHSV 30,000 h^{-1}. The reactor outlet gas composition was analyzed with respect to NO, NO_2, N_2O and CO by a MKS 2000 FTIR instrument. The CO_2 content was measured by an UNOR 610 non-dispersive IR CO_2 analyzer (Maihak). Prior to the experiments the catalyst was pre-treated in 8% O_2 (Ar bal.) at 550 °C for 20 min. Octane was introduced to the reactor via an external controlled evaporator mixer (Bronkhorst), where the octane and carrier gas flows were controlled by mass flow controllers and mixed at constant temperature (25 °C). Experiments with different feed conditions were carried out in series with switching between reactant feed concentrations to allow transient responses to be observed. The feed gas concentrations of NO, O_2, octane, H_2 and the feed temperature were varied systematically between high and low levels of 315–815 ppm, 2–7%, 150–250 ppm, 0.1–1% and 250–350 °C, respectively. The feed gas was in all cases free of water. Table 1 shows the experimental plan, which was a reduced factorial design, but due to practical limitations the design variables were not completely orthogonal. However, the resulting MLR condition number (where an orthogonal design has condition number of unity) was 6.7 which is acceptable for all interpretations below.

Empty reactor step change experiments were performed with NO and NO_2, however CO_2 step changes were used to represent H_2 and O_2 transients. These empty reactor experiments characterized the axial gas dispersion and lag time in the reactor system and were used as the transient feed concentrations for the simulations.

3. Modeling methods

3.1. Monolithic catalyst model

The catalyst monolith model used can be characterized by the following points:

- Parallel channels in the monolith were assumed to be identical.
- Axially the monolith was modelled as 15 "tanks-in-series". The theoretical number of tanks based on an estimate of the axial dispersion was considerably more, but it was found that including additional tanks did not make significant changes in the model results.
- Modeling of mass and heat transfer from the bulk gas to the washcoat surface was performed by a film model. The mass and heat transport coefficients estimated from a correlation [24] in which the Sherwood and Nusselt numbers decreased along the channel axes and approached asymptotic values of 3.
- Variation in the total gas concentration (c_{tot}) due to total mole changes resulting from the reactions was neglected due to the low concentrations of the reactant species. However, the model did account for the influence of temperature variation on c_{tot}.
- From the experimental data, the maximum observed value of the estimated Weisz modulus was 0.93 based on the overall rate of NO reduction at steady state observations. Since Weisz modulus values less than unity indicate the absence of pore transport resistance, transport limitation in the washcoat was neglected.
- Radial temperature gradients within and between the catalyst washcoat and the monolith were neglected. However heat

Table 1
Experimental conditions and results at steady state.

Transient series		Feed conditions						Steady state results		
		NO (ppm)	NO_2 (ppm)	n-C8 (ppm)	H_2 (%)	O_2 (%)	Temperature (°C)	NO_x conversion (%)	n-C8 conversion (%)	NO_x reduction selectivity (mol/mol)
A	1	515	0	150	0	5	300	1.1	9.7	0.4
	2	515	0	150	0.5	5	300	30.8	60.4	1.8
	3	415	100	150	0.5	5	300	28.3	55.5	1.8
	4	315	200	150	0.5	5	300	27.6	57.3	1.7
	5	315	200	150	0	5	300	0.2	11.5	0.1
B	1	315	0	150	0	2	250	0.0	3.3	0
	2	315	0	150	1	2	250	50.7	43.0	2.5
	3	815	0	150	0.1	2	250	3.1	4.0	4.1
	4	815	0	150	1	7	250	22.8	60.3	2.1
	5	315	0	150	0.1	7	250	27.0	15.8	3.6
C	1	315	0	150	1	7	350	30.9	56.5	1.2
	2	315	0	150	0.1	2	350	19.2	34.9	1.2
	3	815	0	150	1	2	350	16.2	45.5	1.9
	4	815	0	150	0.1	7	350	10.8	43.3	1.4
D	1	315	0	250	0	2	350	3.8	21.3	0.2
	2	315	0	250	1	2	350	31.0	45.7	0.9
	3	815	0	250	0.1	2	350	7.7	27.1	0.9
	4	315	0	250	0.1	7	350	37.7	53.1	0.9
	5	815	0	250	1	7	350	21.1	55.8	1.2
E	1	815	0	250	0.1	7	250	6.8	3.7	6.2
	2	315	0	250	1	7	250	60.0	62.6	1.2
	3	315	0	250	0.1	2	250	12.0	2.6	5.9

transport resistance between the monolith and the quartz tube in which it was contained was included in the model. The quartz tube was assumed to be at a uniform temperature and heat transport from the quartz tube to the surroundings was neglected.
- Physical properties such as the heat capacities, thermal conductivities and diffusivities were assumed to be constant and were estimated for an average gas composition and average temperature of 300 °C.

It was found that due to the high space velocity used in the experiments, mass and heat accumulation in the bulk gas could be neglected without influencing the model result. Thus in each tank the mass balance for each component and heat balance in the gas bulk was:

$$F_{tot}(y_f - y_b) - k_c a(y_b - y_s)c_{tot} = 0 \quad \text{(i)}$$

$$F_{tot}c_{Pgas}(T_f - T_b) - ha(T_b - T_s) = 0 \quad \text{(ii)}$$

In each tank the mass balance for each adsorbed component and the heat balance in the catalyst washcoat were:

$$\frac{d\theta}{dt} = \sum_i^{n_{rxn}} \chi_i r_i \quad \text{(iii)}$$

$$\frac{dT_s}{dt} = \frac{\sum_i^{n_{rxn}}(-\Delta H_{Ri})r_i N m_{\tan k} - ha(T_s - T_g) - UA(T_s - T_p)}{c_{Pmono}m_{mono}} \quad \text{(iv)}$$

The following balance was applied between the surface reaction rate and the mass transport of each species in each tank between bulk gas and surface:

$$\sum_i^{n_{rxn}} \upsilon_i r_i N m_{\tan k} + k_c a(y_b - y_s)c_{tot} = 0 \quad \text{(v)}$$

Finally the heat balance for the quartz tube was:

$$\frac{dT_p}{dt} = \frac{\sum_i^{n_{\tan k}} UA(T_{si} - T_p)}{c_{Pp}m_p} \quad \text{(vi)}$$

The value of the heat transport coefficient between the monolith and the quartz tube (UA) was manually tuned in order to reproduce the shape of the experimental temperature transients (in this case $UA = 0.01\ W\ K^{-1}$). Reaction enthalpies (ΔH_R) were estimated using the following criteria:

- Enthalpies of reversible elementary reactions were set equal to the differences in their activation energies.
- Enthalpies of irreversible reactions that produced only surface intermediate species were set equal to zero.
- Enthalpies of irreversible reactions that produced final products (adsorbed or in gas phase) were calculated from enthalpies of the overall reactions in Table 2 with corrections made for adsorbed species based on their enthalpies of adsorption (from adsorption/desorption activation energies).

The result is that the enthalpy of every surface reaction was not exactly estimated, however more importantly, the global overall reaction enthalpies were correct. The resulting system of algebraic and ordinary differential equations (Eqs. (i)–(vi) expanded for each tank, gas phase and adsorbed species) was numerically solved using the ode15s function in MATLAB 7.1.

3.2. Kinetic model parameter fitting

The kinetic model is presented in Section 5 below. An objective of the modelling was to estimate the kinetic parameters based on the

Table 2
Overall reactions used to estimate reaction enthalpies.

Overall reaction	Reaction enthalpy ($J\ mol^{-1}$) at 300 °C
$2NO + (1/8)C_8H_{18} + 0.0625O_2 \rightarrow N_2 + CO + 1.125H_2O$	-5.469×10^5
$0.125C_8H_{18} + 1.0625O_2 \rightarrow CO + 1.125H_2O$	-3.559×10^5
$CO + 0.5O_2 \rightarrow CO_2$	-2.856×10^5
$NO + 0.5O_2 \rightarrow NO_2$	-6.320×10^4
$H_2 + 0.5O_2 \rightarrow H_2O$	-2.478×10^5
$2NO_2 + (1/8)C_8H_{18} + 0.0625O_2 \rightarrow 2NO + CO + 1.125H_2O$	-2.295×10^5

experimental results. In order to avoid correlation between the pre-exponential factors (A_i) and activation energies (E_{Ai}), the rate constant ($k_{m,i}$) at an average temperature (T_m) of 300 °C and the activation energy were used as fitting parameters. Thus for parameter fitting purposes the Arrhenius equation was reformulated as

$$k_i = k_{m,i}\exp\left(\frac{E_{Ai}}{R}\left(\frac{1}{T_m}-\frac{1}{T}\right)\right)$$

where k_i is the rate constant at temperature T.

Parameter fitting was performed using a gradient search method with the objective function of minimizing the residual sums of squares for the measured concentrations of NO, NO_2, CO_2, CO and the outlet temperature. The function lsqnonlin in MATLAB 7.1 was used with lower and upper bounds for the scaled parameter values. The parameter scaling methods are described elsewhere [25].

4. Experimental results

Table 1 shows the transient series (5 in total) of experimental conditions run. Each set of conditions (22 in total) was run for 20–30 min. In most cases this time period was sufficient to reach steady state. The results included in Table 1 are only the steady state conversions and NO_x reduction selectivity for each set of conditions. The NO_x reduction selectivity is the ratio of moles of NO_x converted to the moles of carbon in n-octane consumed (i.e. moles NO_x converted/moles n-octane consumed × 8). The n-C8 conversion is the conversion of n-octane to CO and CO_2. Fig. 1 shows a portion (transient series A) of the experimentally observed outlet transient concentrations and temperatures. For all experimental conditions the N_2O yield was low, with outlet concentrations typically less than 15 ppm.

4.1. Influence of NO_2/NO feed ratio

In transient series A, experiments were carried out to investigate the influence of the feed ratio of NO_2/NO while the total NO_x feed concentration was constant at 515 ppm. Both with and without hydrogen, an increase in the NO_2/NO feed ratio caused a slight decrease in the NO_x conversion (see Table 1). The NO_2 yield also decreased with higher NO_2/NO feed ratio, indicating that NO_2 was readily converted, however largely to NO. For example, Fig. 1 shows that for experiments 4 and 5 of transient A, the NO outlet concentrations reached 325 and 457 ppm, respectively, both higher than the inlet concentrations (315 ppm). There is thus no indication that NO_x reduction occurs more readily with NO_2. It has been reported previously that NO_2 is less readily reduced to N_2 compared to NO with propane reductant [7]. In addition for experiments 3–5 of transient A, when NO_2 is added to the feed, the outlet NO_2 concentration is always far less than what would be expected for if the NO oxidation reaction ($NO + 0.5O_2 \leftrightarrow NO_2$) were to reach equilibrium at the outlet experimental conditions. For example for experiment 4 the outlet NO_2 concentration was 48 ppm whereas if the NO oxidation reaction reached equilibrium the NO_2 concentration would have been 195 ppm. There are apparently other reactions involved that consume NO_2 and this is the case both with and without the addition of hydrogen. In experiments 1 and 5 of transient A, without feed of hydrogen when the NO_x conversion is very low, the n-octane conversion increased with the NO_2/NO feed ratio. It is thus likely that n-octane contributes to the reduction of NO_2 to NO.

4.2. Influence of reactant feed concentrations and temperature

The steady state experiments provide information to determine the influence of NO, n-octane, H_2, O_2 feed concentrations and temperature on the steady state conversions and selectivity. The

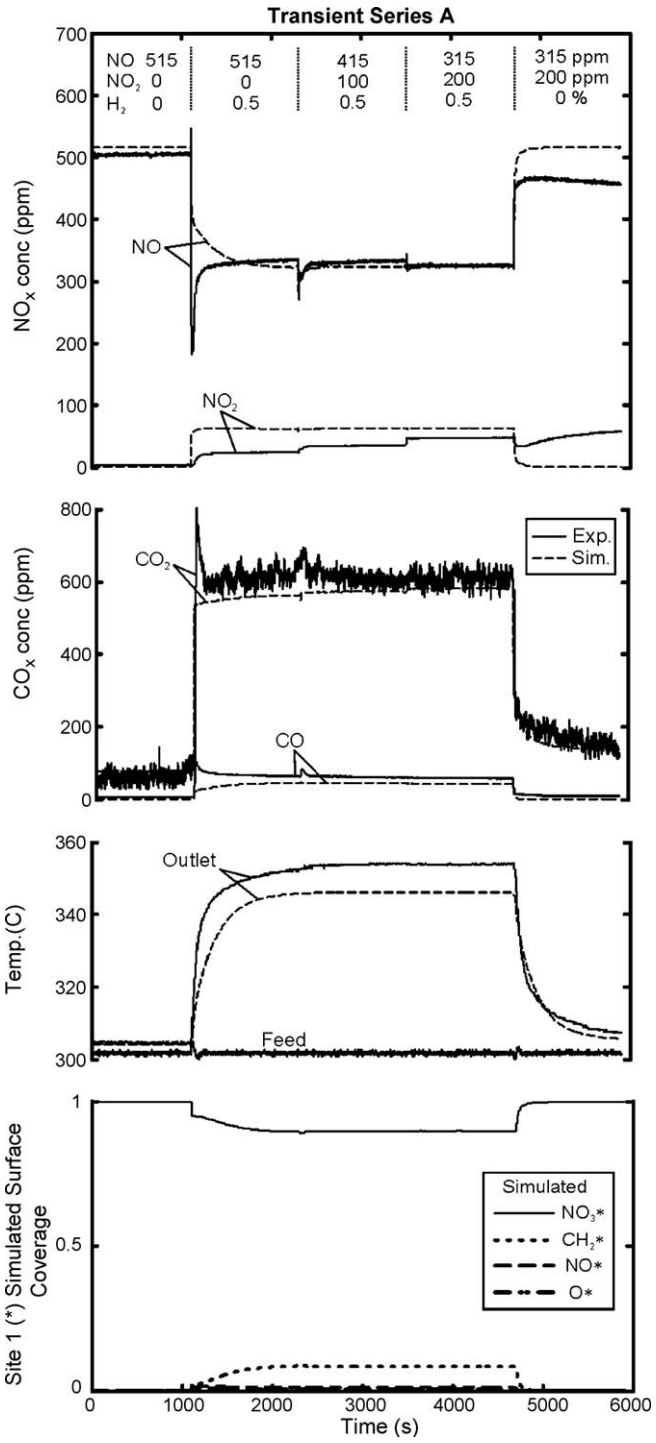

Fig. 1. Transient series A experimental and simulation results with varying feed concentrations of NO, NO_2 and H_2. Constant feed conditions: 300 °C, 5% O_2, 150 ppm n-octane.

data was analyzed by fitting a multivariate linear regression (MLR) model with feed concentrations and temperature as variables and NO_x conversion, n-octane conversion and NO_x reduction selectivity as responses. Fig. 2 shows the MLR model coefficients for each response variable. The coefficients describe the change in the response variable when the parameter (i.e. a feed concentration or temperature) is increased from its centre level to high level. The experimental data and MLR model could also give information about two-way interactions between parameters or quadratic effects. The only second order terms found to be non-negligible

was that between hydrogen and temperature (Temp × H_2), temperature (Temp × Temp) and hydrogen ($H_2 \times H_2$), and thus these are included in Fig. 2. Generally the influence of the feed conditions was largely in agreement with reports in the literature with other silver alumina catalysts with n-octane or other hydrocarbon reductants.

Increasing the H_2 feed concentration clearly increased both the NO_x and n-octane conversion. However hydrogen feed had a negligible influence on the NO_x conversion selectivity indicated by its small coefficient value and large confidence interval that symmetrically straddles the zero coefficient value. Hydrogen's ability to clearly activate the NO_x reduction reaction at temperatures below about 400 °C is widely reported in the literature [26]. Fig. 1 shows that these effects of the addition (transient for first feed switch) or removal (transient for final feed switch) of hydrogen occur quickly, mostly over a few seconds as observed also by others [27]. The addition of hydrogen also, as seen in Fig. 1, caused an increase in the outlet temperature of about 50 °C. For all experiments the outlet temperature was from 3 to 105 °C higher than the inlet, but the particularly high outlet temperatures corresponded to experiments with feed of hydrogen. By using the enthalpies of the overall reactions in Table 2 and assuming the reactor was adiabatic, it was possible to estimate that the hydrogen conversions to water at steady state mostly ranged from 30% to 60%. Certainly part of the positive effect of hydrogen addition on NO_x conversion can be attributed to increasing the temperature due to its own oxidation, however this is a fact that is seldom pointed out in the literature. It was also found that the quadratic hydrogen concentration ($H_2 \times H_2$) was significant and it reduced the NO_x conversion, octane conversion and the NO_x conversion selectivity. This is because the hydrogen concentration has a nonlinear effect, i.e. its positive influence on activating the NO_x reduction and hydrocarbon conversion diminishes at higher concentrations which has also been experimentally observed by others with propane reductant [15].

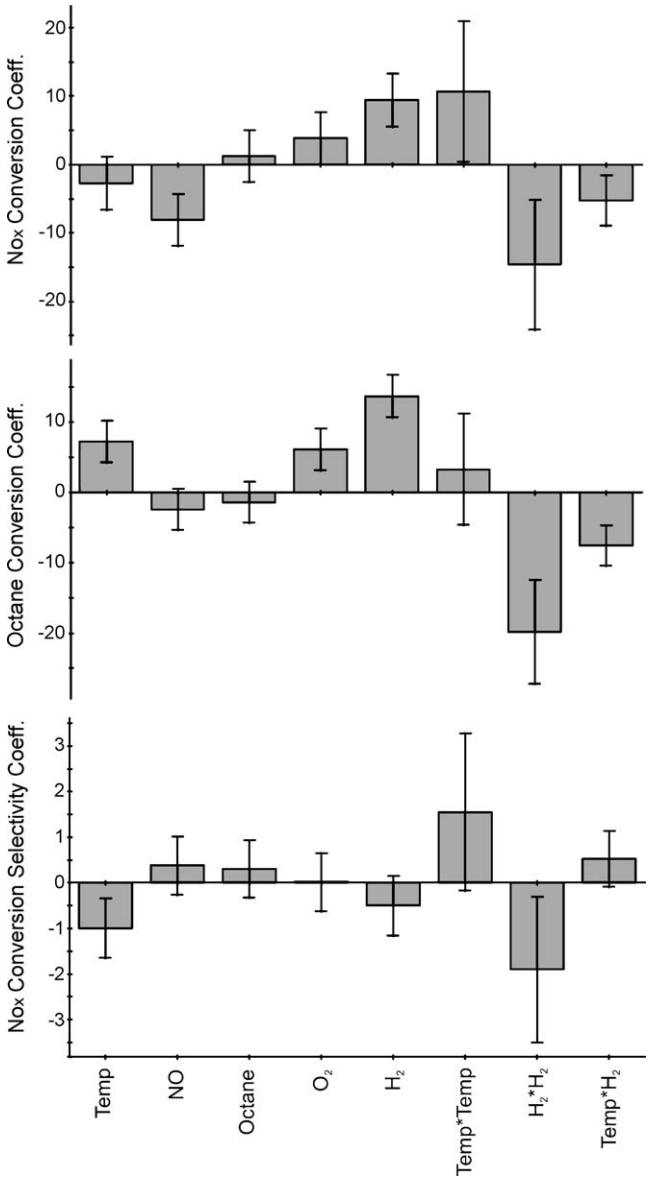

Fig. 2. Coefficient plot for the MLR model. Columns are coefficient values with bars indicating 95% confidence intervals. The explained variance (R^2) for the three responses was 0.89, 0.96 and 0.70, respectively.

An increased feed concentration of NO clearly decreased the NO_x conversion, but had negligible effects on the n-octane conversion and the NO_x reduction selectivity (see Fig. 2). An apparent poisoning effect of NO for NO_x conversion has previously been observed with n-octane [2,8], n-hexane [28] and propane [15,29] as the reductants and it supports the suggestion that nitrate species block the catalyst surface.

An increased oxygen concentration caused a clear increase in n-octane conversion, a smaller increase in NO_x conversion, but had no effect on the NO_x reduction selectivity (see Fig. 2). In the literature it has been found that oxygen inhibits NO_x reduction [8] with hydrogen present whereas in the absence of hydrogen, NO_x reduction is promoted [2] with n-octane as the reductant. In a study with propane reductant, Shimizu et al. [15] found that NO_x reduction was strongly promoted by oxygen in the absence of hydrogen, however the effects of oxygen were small with hydrogen present. Furthermore, under all conditions higher oxygen concentrations increased the rate of hydrocarbon oxidation. It may well be that oxygen may both promote and inhibit NO_x reduction depending on the conditions. It has been widely proposed that oxygen's role is to activate hydrocarbons to form partially oxidized species such as acetate [10,15,27,30,31]. But on the other hand, if nitrates should poison the catalyst surface, oxygen may promote the oxidation of NO_x adspecies to nitrate poisons or higher oxidation concentrations may promote the non-selective complete oxidation of hydrocarbon reductants.

The n-octane feed concentration (HC) had little influences on the NO_x and n-octane conversion and NO_x reduction selectivity (see Fig. 2). In other studies it has been reported that with both n-octane and propane reductants, an increased hydrocarbon concentration promotes both NO_x reduction and hydrocarbon conversion [2,8,15]. In these other studies the experimental space was much smaller and the levels were different, whereas in the present study an interest in the influence of many different factors was balanced against a desire for a manageable number of experiments. To clearly determine its effects, the n-octane concentration was likely not varied over a wide enough range in the present experimental study.

According to the MLR model, higher temperature caused a small reduction in NO_x conversion, a larger and more significant increase in n-octane conversion and a decrease in NO_x reduction selectivity. It has been found previously that NO_x reduction selectivity can decrease with temperature, but this typically occurs at temperatures exceeding about 400 °C [28,32]. Higher temperature may favour the non-selective direct oxidation of the hydrocarbon and/or hydrogen. It is not surprising that the quadratic temperature term (Temp × Temp) has a positive effect on the responses since temperature should have a nonlinear influence on reaction rates as an Arrhenius relationship predicts.

The only two-way interaction term between temperature and hydrogen (Temp × H_2) was significant. From Fig. 2 it can be seen that increasing both temperature and hydrogen together reduced the NO_x conversion and n-octane conversion and caused a small increase in the NO_x reduction selectivity. This may occur because higher temperature favours the direct oxidation of hydrogen, so that hydrogen's normally favourable influence on NO_x reduction and n-octane conversion is partially lost.

5. Kinetic modeling

The complete kinetic model is a mean field model consisted of 23 reactions involving 7 gas phase species and 8 surface species on 2 catalytic sites. The model reactions and rate expressions are listed in Tables 3–6. The kinetic model accounted for adsorption/desorption of gas phase species and surface reactions. Surface reactions involving NO_x adspecies are elementary, whereas most others are overall reactions.

Table 3 lists the adsorption and desorption reactions on the main catalytic site, site 1 (*). The pre-exponential factors for adsorption in all cases were calculated from kinetic gas theory [33] at the average experimental temperature of 300 °C with an assumed site area of 8×10^{-20} m^2 $site^{-1}$ [34] and a sticking coefficient at zero coverage of 0.1. The pre-exponential factors for desorption were set to 10^{13} s^{-1}. The activation energy for adsorption of all gaseous species was set to zero. Further to reduce the number of adjustable parameters, the activation energy for oxygen desorption was taken from [35] and the activation energy for NO desorption was set to 120 kJ mol^{-1}, taking into account the gas phase enthalpy and a reasonable binding energy.

Table 4 lists the surface reactions involving NO_x adspecies on site 1 (*). Adsorbed NO is oxidized to both NO_2* and NO_3* surface species. A thermodynamic constraint for the gas phase NO oxidation reaction ($NO + 0.5O_2 \leftrightarrow NO_2$) was imposed. This involved the use of the enthalpy and entropy changes for gas phase NO oxidation at the average experimental temperature (300 °C) to constantly adjust parameter values for reaction (9) (k_9, E_{A9}) during parameter fitting based on the current parameter values for reactions (1)–(6) and (10). The adsorbed nitrate species (NO_3*) formed in reaction (11) build up in the absence of hydrogen to cover site 1 (*) and prevent NO_x reduction. In reaction (12), gas phase hydrogen reacts with nitrates via an Eley Rideal type reaction to form NO_2* species which are subsequently reduced to N_2. It was found necessary to have hydrogen react with nitrates directly from the gas phase and not via a dissociative adsorption step in order to rapidly clear site 1 of nitrates and gain NO_x reduction activity with the introduction of hydrogen as experimentally observed. At elevated temperature it should be possible for the reverse of reaction (11) to occur, i.e. nitrate decomposition to free up site 1, since Ag/Al_2O_3 catalysts are active for NO_x reduction in the absence of hydrogen at higher temperatures. The reverse of reaction (11) was not included in the kinetic model because at the experimental range of temperature used, the NO_x conversion was low (always less than 4%) for the few experiments without hydrogen feed and as a result significant values for nitrate decomposition could not be obtained.

Table 5 contains the surface reactions leading to NO_x reduction and oxidation of n-octane. All of these reactions, except reaction (16), are non-elementary. First in reaction (13), n-octane reacts with surface oxygen to form CH_2* surface species, since it has been widely proposed in the literature that the role of oxygen is to activate the hydrocarbon reductant [36]. In reality the CH_2* species may be partially oxidized surface hydrocarbon fragments of varying carbon chain length. Partially oxidized hydrocarbon species have been proposed in the literature as reaction intermediates. In the simple overall reaction (14), NO_2* is reduced to nitrogen, whereas the non-selective oxidation of surface hydrocarbons is accounted for by reaction (15). Surface CO* species produced by reactions (14) and (15) may desorb to the gas phase or be further oxidized to CO_2 in reaction (16). A reaction pathway for direct NO_x reduction by hydrogen, analogous to reaction (14), is not included in the kinetic model because it has been shown in the experimental literature that hydrogen alone does not act as a reducing agent for NO_x reduction but instead as a strong promoter of hydrocarbon SCR [5,8,37]. In addition N_2O formation is neglected in the kinetic model since its concentrations in the experiments were always low.

The various other adsorption/desorption and oxidation reactions (reactions (17)–(23)) occurring on site 2 (#) are listed in Table 6. The surface reactions (21) and (22) are non-elementary. These reactions must occur on a second site because some catalytic

Table 3
Reactions and rate expressions for adsorption/desorption on site 1 (*).

Reaction		Rate expression
$NO + * \rightarrow NO*$	(1)	$r_1 = k_1 P_{NO*} \theta_*$
$NO* \rightarrow NO + *$	(2)	$r_2 = k_2 \theta_{NO*}$
$O_2 + 2* \rightarrow 2O*$	(3)	$r_3 = k_3 P_{O_2} \theta_*^2$
$2O* \rightarrow O_2 + 2*$	(4)	$r_4 = k_4 \theta_{O*}^2$
$NO_2 + * \rightarrow NO_2*$	(5)	$r_5 = k_5 P_{NO_2} \theta_*$
$NO_2* \rightarrow NO_2 + *$	(6)	$r_6 = k_6 \theta_{NO_2*}$
$CO + * \rightarrow CO*$	(7)	$r_7 = k_7 P_{CO} \theta_*$
$CO* \rightarrow CO + *$	(8)	$r_8 = k_8 \theta_{CO*}$

Table 4
Reactions and rate expressions for NO_x adspecies on site 1 (*).

Reaction		Rate expression
$NO* + O* \rightarrow NO_2* + *$	(9)	$r_9 = k_9 \theta_{NO*} \theta_{O*}$
$NO_2* + * \rightarrow NO* + O*$	(10)	$r_{10} = k_{10} \theta_{NO_2*} \theta_*$
$NO_2* + O* \rightarrow NO_3* + *$	(11)	$r_{11} = k_{11} \theta_{NO_2*} \theta_{O*}$
$H_2 + NO_3* \rightarrow H_2O + NO_2*$	(12)	$r_{12} = k_{12} \theta_{NO_3*} P_{H_2}$

Table 5
Reactions and rate expressions for surface reactions on site 1 (*).

Reaction		Rate expression
$C_8H_{18} + O* + 7* \rightarrow 8CH_2* + H_2O$	(13)	$r_{13} = k_{13} P_{oct} \theta_{O*}^2 \theta_*$
$CH_2* + 2NO_2* \rightarrow N_2 + CO* + 2O* + H_2O$	(14)	$r_{14} = k_{14} \theta_{CH_2*} \theta_{NO_2*}$
$CH_2* + 2O* \rightarrow CO* + 2* + H_2O$	(15)	$r_{15} = k_{15} \theta_{CH_2*} \theta_{O*}$
$CO* + O* \rightarrow CO_2 + 2*$	(16)	$r_{16} = k_{16} \theta_{CO*} \theta_{O*}$

Table 6
Reactions and rate expressions for adsorption/desorption and oxidation reactions on site 2 (#).

Reaction		Rate expression
$O_2 + 2\# \leftrightarrow 2O\#$	(17)	$r_{17} = k_{17} P_{O_2} \theta^2$
$2O\# \rightarrow O_2 + 2\#$	(18)	$r_{18} = k_{18} \theta_O^2$
$NO_2 + \# \rightarrow NO_2\#$	(19)	$r_{19} = k_{19} P_{NO_2} \theta$
$NO_2\# \rightarrow NO_2 + \#$	(20)	$r_{20} = k_{20} \theta_{NO_2}$
$C_8H_{18} + 25O\# \rightarrow 8CO_2 + 25\# + 9H_2O$	(21)	$r_{21} = k_{21} P_{oct} \theta_O$
$C_8H_{18} + 25NO_2\# \rightarrow 8CO_2 + 25NO + 9H_2O + 25\#$	(22)	$r_{22} = k_{22} P_{oct} \theta_{NO_2}$
$H_2 + O\# \rightarrow H_2O + \#$	(23)	$r_{23} = k_{23} \theta_O P_{H_2}$

activity for octane oxidation by oxygen (reaction (21)) or NO_2 (reaction (22)) was experimentally observed in the absence of hydrogen when site 1 (*) was largely poisoned by nitrates. As a result most of these reactions (17)–(22) have only a minor influence when hydrogen is present. The oxidation of octane by NO_2 in reaction (22) is necessary to account for the high activity for NO_2 reduction observed in the transient series A experiments, with NO_2 conversions beyond the thermodynamic limitations for the NO oxidation reaction ($NO + 0.5O_2 \leftrightarrow NO_2$), discussed above. Finally direct hydrogen oxidation (reaction (23)), not involving NO_x adspecies, also occurs on site 2. It has been proposed in the literature that well dispersed Ag^+ species, more predominant in catalyst samples with low loadings of silver, are active for NO_x reduction whereas large silver metallic species that dominate at higher loading or low dispersion are active for the combustion of hydrocarbons [28,38,39]. Sites 1 and 2 used in this kinetic model may be considered to correspond to Ag^+ species and metallic silver, respectively. As reported in a previous publication [21], it was found that a sample prepared by a sol–gel method, identical to that used for the sample in this study, contained more silver of higher oxidation state than a sample prepared by impregnation. The presence of metallic silver could not be detected by X-ray diffraction on the freshly prepared sol–gel sample, however this does not rule out the possibility that the sample contains small amounts of metallic silver or that it can be formed during the reaction conditions.

6. Discussion

Table 7 shows the fitted and fixed parameter values as well as the 95% confidence intervals for the fitted parameters. In most cases the confidence intervals are small compared to the magnitude of the parameter values. Only the values for k_{12} and E_{22} appear to be poorly defined by the experimental data, based on the confidence intervals. The fitted value for the site density for site 1 (*) was $0.0260 \pm 9.03 \times 10^{-4}$ mol (kg cat.)$^{-1}$ which corresponds to 7.9% of the total silver loading. Most of the reactions occurring on site 2 (#) have only a minor influence when hydrogen is present as is the case for most of the experimental data. Due to the lesser importance of site 2 (#), particularly for the transient responses, its density was not fitted but instead fixed arbitrarily to a value corresponding to 20% of the silver loading. The actual proportion of the silver loading as site 2 may be much lower if it represents metallic silver, since metallic silver has been found to be scarce on sol–gel prepared $Ag–Al_2O_3$ [21]. Note that even though the confidence intervals are relatively small, the systematic deviations (often referred to as Lack-of-Fit) are in some cases substantial. The magnitude of the confidence intervals is still a valuable measure of which part of the mechanism requires more targeted experiments for improved fit.

6.1. Hydrogen effect and nitrate coverage

Figs. 1, 3 and 4 compare the experimental and simulation results for each transient series of experiments. The most extreme transient responses occur of course when hydrogen is introduced, such as the first feed switches in transient series A, B and D, when

Table 7
Fitted parameter values and 95% confidence intervals.

Reaction	Rate constants			Activation energies	
	$\ln(k_{m,i})$	Units	Confidence interval	E_{Ai} (kJ mol^{-1})	Confidence interval
(1)	13.57	m^3 s^{-1} mol^{-1}	Fixed	0	Fixed
(2)	4.75	s^{-1}	Fixed	120	Fixed
(3)	13.52	m^3 s^{-1} mol^{-1}	Fixed	0	Fixed
(4)	−1.55	s^{-1}	Fixed	150	Fixed
(5)	13.33	m^3 s^{-1} mol^{-1}	Fixed	0	Fixed
(6)	5.88	s^{-1}	Fixed	114.6	±0.488
(7)	13.58	m^3 s^{-1} mol^{-1}	Fixed	0	Fixed
(8)	9.34	s^{-1}	Fixed	98.1	±1.439
(9)	6.18	s^{-1}	Constrained[a]	296.0	Constrained[a]
(10)	12.34	s^{-1}	±0.1005	278.8	±3.019
(11)	7.956	s^{-1}	±0.0736	182.8	±2.096
(12)	−0.0238	m^3 s^{-1} mol^{-1}	±0.0464	44.5	±2.638
(13)	14.06	m^3 s^{-1} mol^{-1}	±0.0859	207.7	±2.734
(14)	5.565	s^{-1}	±0.0668	12.7	±1.702
(15)	2.291	s^{-1}	±0.0589	2.19	±1.947
(16)	9.292	s^{-1}	±0.2798	212.1	±1.780
(17)	13.52	m^3 s^{-1} mol^{-1}	Fixed	0	Fixed
(18)	−1.552	s^{-1}	Fixed	150	Fixed
(19)	13.34	m^3 s^{-1} mol^{-1}	Fixed	0	Fixed
(20)	5.732	s^{-1}	Fixed	115.3	±1.469
(21)	−2.012	m^3 s^{-1} mol^{-1}	±0.0169	71.7	±0.752
(22)	7.180	m^3 s^{-1} mol^{-1}	±0.3026	0.00	±1.782
(23)	−0.3894	m^3 s^{-1} mol^{-1}	±0.0357	9.32	±1.263

[a] Values obtained from thermodynamic constraint imposed on gas phase NO oxidation ($NO + O_2 \leftrightarrow NO_2$) on site 1.

the feed concentration of hydrogen is increased from 0% to 0.5% or 1%. In all of these cases the NO_x and hydrocarbon conversion and outlet temperature increases quickly. According to the model this occurs because without hydrogen, site 1 is completely covered by NO_3* species. Hydrogen reduces the NO_3* species to NO_2* by reaction (12) which can be subsequently reduced to N_2. Clearing some of the catalytic sites of NO_3* also allows oxygen adsorption and subsequently hydrocarbon species (CH_2*) to accumulate on the catalyst surface which are either directly oxidized (reaction (15)) or act as reductants for NO_2* (reaction (14)). The temperature increases partially due to the increased rates of NO_x reduction and hydrocarbon oxidation, but mostly due to hydrogen oxidation. Hydrogen is oxidized either by NO_3* (reaction (12)) or O# (reaction (23)) surface species, however according to the modeling results the oxidation of hydrogen by surface oxygen species accounts for the larger part of the temperature increase. The model transient responses are at about the correct time scale as the experimental data, however at lower temperatures (transients A and B), the NO concentration first quickly decreases, but then continues to decrease but at a slower rate, probably due to slower changes in surface coverages. When the feed of hydrogen is discontinued in the last feed switch in transient series A, the reverse process occurs where the NO_x reduction, hydrocarbon conversion and outlet temperature all quickly decrease. Again, for the reverse process the predicted transient responses occur over about the same time scale as the experimental results.

6.2. Feed concentration effects and interactions

Generally according to the kinetic model (Tables 3–6), increased concentrations of NO and decreased concentrations of hydrogen should cause a decreased rate of NO_x reduction and an increased rate of hydrocarbon oxidation. These effects were also apparent in the experimental data according to the MLR model (see Fig. 2). An increase in the NO concentration can cause a higher concentration of NO_x adspecies including the NO_3* poison (reactions (9) and (11)). Also, a decrease in the concentration of hydrogen would decrease the rate of reduction of the NO_3* poison. In the second feed switch of transient series C, the feed concentrations of NO and hydrogen were increased. In this case the effect of hydrogen is apparently far greater on the NO_3* surface concentration because the model predicts that it decreases strongly. However, the opposite is true in the fourth feed switch of transient series B. Under the conditions of this experiment, NO has a greater influence on the NO_3* surface concentration because it moderately decreases. The differences in the influence of NO and H_2 between these feed switches (second in series C and fourth in series B) lies partly in the different feed temperatures, but more so

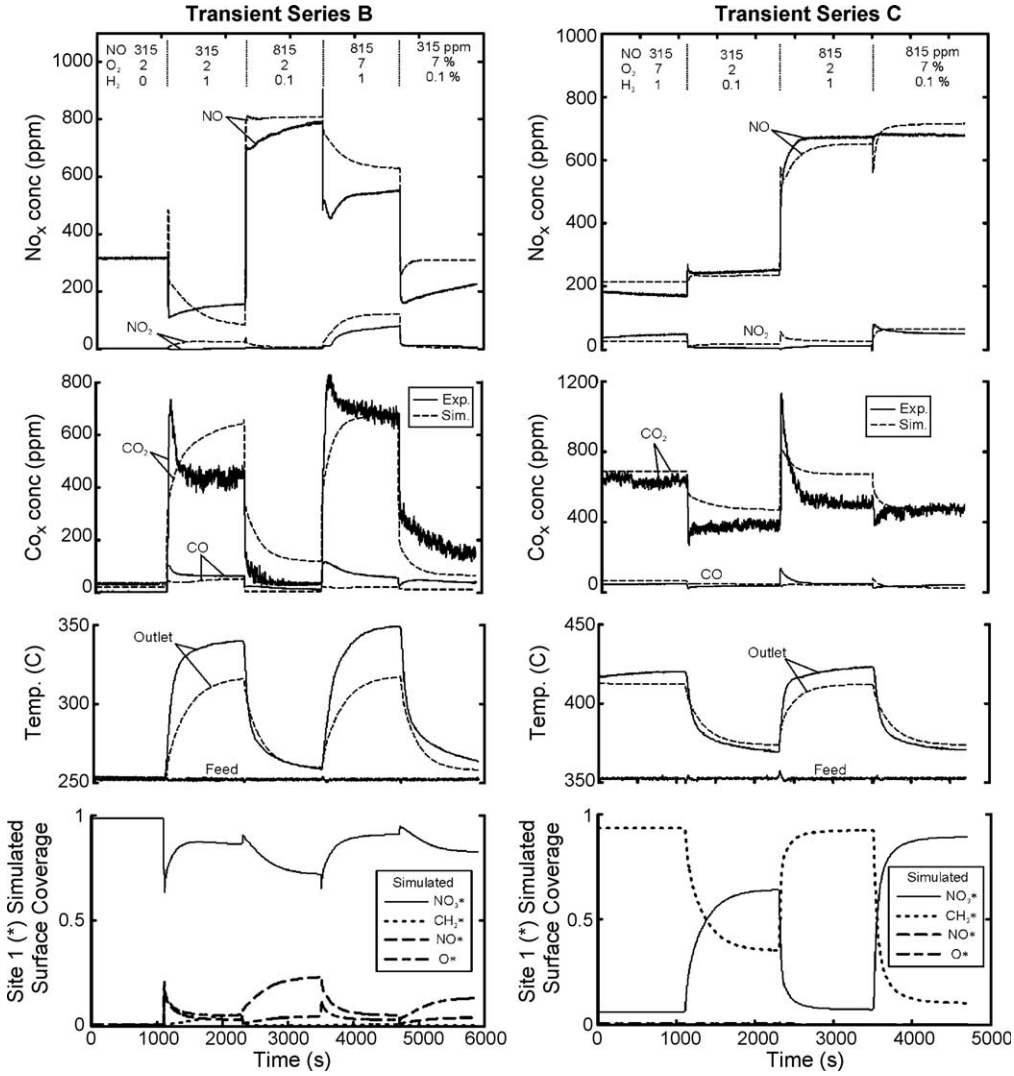

Fig. 3. Transient series B (left) and C (right) experimental and simulation results with varying feed concentrations of NO, O_2 and H_2. Constant feed conditions: 250 °C (transient B), 350 °C (transient C) and 150 ppm n-octane.

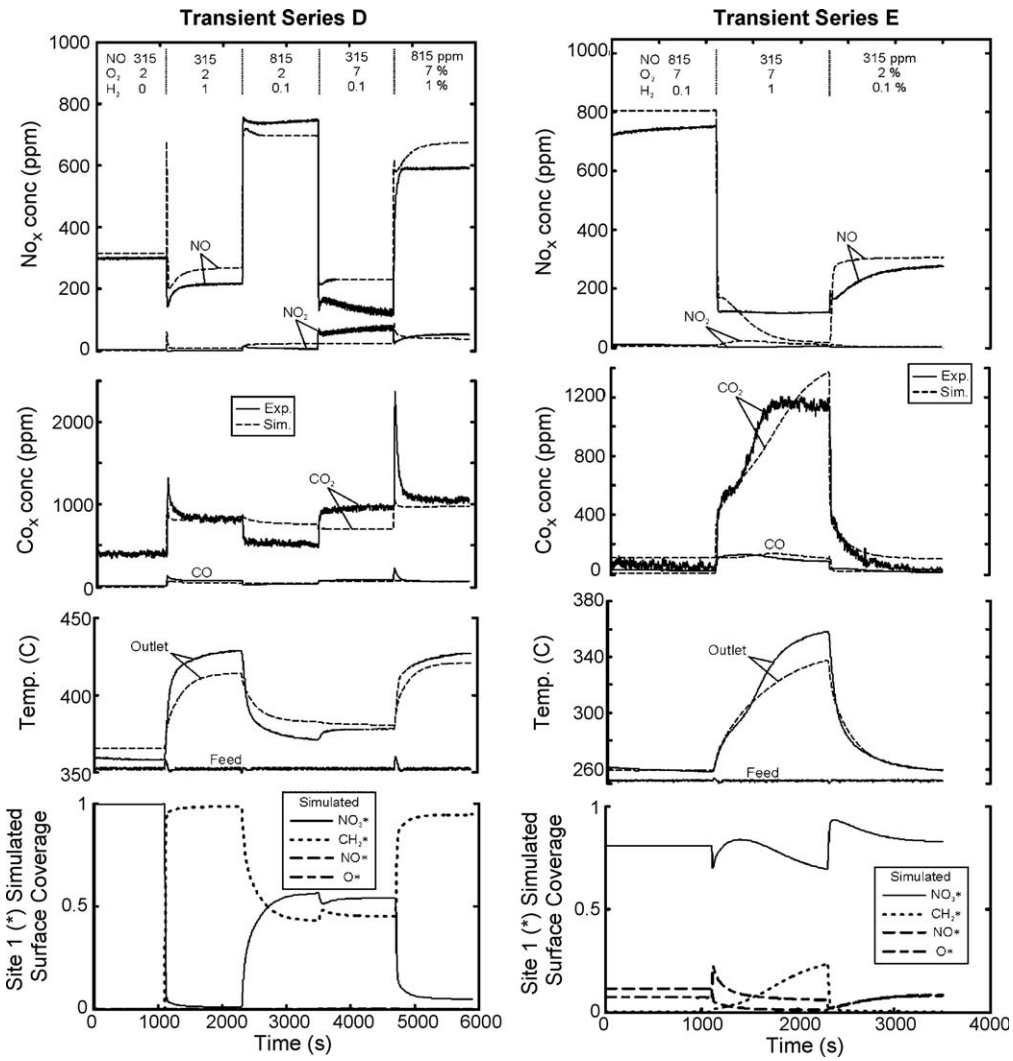

Fig. 4. Transient series D (left) and E (right) experimental and simulation results with varying feed concentrations of NO, O_2 and H_2. Constant feed conditions: 350 °C (transient D), 250 °C (transient E) and 250 ppm n-octane.

in the different oxygen concentrations. The higher oxygen concentration in the switch in series B would also promote the formation of NO_3* surface species which causes changes in the NO concentration to be more influential instead of hydrogen. Also, for both of these feed switches the model predicts the correct change in the NO_x conversion (increasing for the switch in series B whereas decreasing for the switch in series C) although the NO_x concentrations are clearly better predicted in series C.

In the second feed switch of transient series B, the surface concentration of NO_3* decreases despite the fact that the NO feed concentration increased and hydrogen decreased. This change in NO_3* concentration is unexpected if one only considers the fact that NO contributes to NO_3* formation whereas H_2 removes it. The model predicted a large decrease in the NO_x conversion like that experimentally observed, however in this case it results from other secondary effects such as the reduction in the outlet temperature. Also, although the NO_3* concentration does not increase, the NO* concentration does increase due to lower temperature and higher NO feed concentration. In this case, the low n-octane feed concentration (150 ppm) combined with the low oxygen feed (2%) results (via reaction (13) in Table 5) in a lack of surface hydrocarbon species to reduce the increased feed of NO.

In the third feed switch in transient series D, the feed concentration of hydrogen is constant whereas the feed concentrations of NO and oxygen are changed. In this case the surface concentration of NO_3* decreases slightly due to the reduction in the concentration of NO. The reason for the small change in NO_3* concentration is due to the fact that the oxygen concentration also increases and oxygen promotes NO_3* formation. However, at the same time a higher oxygen concentration promotes the formation of CH_2* surface species via reaction (13) and as a result the CH_2* surface concentration also increased slightly. As a result, according to the kinetic model, oxygen should hinder NO_x reduction by enabling NO_3* formation, but on the other hand promote NO_x reduction by enabling the formation of the surface reductant species (CH_2*) via reaction (13). These opposing influences of oxygen are equivalent to the weak although positive effect that oxygen had on the NO_x conversion according to the MLR model (see Fig. 2). In order for the oxygen concentration to modestly increase the rate of NO_x reduction, it was necessary to make reaction (13) second order with respect to the surface oxygen coverage, otherwise changes in oxygen concentration had too strong a relative influence on the concentrations of NO_x adspecies via reactions (9)–(11) (all first order with respect to oxygen surface coverage). It is reasonable to allow reaction (13) to have a higher order dependence on the oxygen surface coverage since it is far from an elementary reaction and due to the simplicity of the model, it can be considered to account for the formation of various oxygenated surface intermediate species.

6.3. Influence of NO/NO_2 feed ratio

Note that in the kinetic model used (reaction (14)) NO_2^* surface species are reduced to nitrogen. An alternative kinetic model was also examined involving NO* in reaction (14), however it was found that having NO_2^* species reduced to nitrogen achieved an overall better fit to the experimental results. The role of NO_2 on NO_x reduction with Ag/Al_2O_3 catalysts has been an issue of some discussion in the literature [38]. It has been reported that NO_2 is not as readily reduced as NO [7] and in agreement with the experimental results presented here, the rate of NO_x reduction decreases when NO_2 is substituted for NO in the feed [5]. These findings suggest the NO_2 or NO_2^* are not important intermediates for NO_x reduction. However, it has also been proposed that NO_2 is an intermediate for NO reduction because it has been observed to be produced more at higher space velocities or at the front part of an Ag/Al_2O_3 catalyst bed and the NO_2 concentration decreases once the formation of N_2 begins [40]. In the kinetic model presented here, a higher NO_2 concentration can both reduce NO_x reduction by promoting NO_3^* formation (reaction (11)), but also it adsorbs to become the intermediate for N_2 formation (reaction (14)). Consequently in transient series A (second and third feed switches), when NO_2 is increasingly substituted for NO in the feed the predicted NO_3^* concentration and NO_x conversion are almost constant, whereas the experimental NO_x conversion only decreased slightly.

6.4. Outcomes from applying an experimental design

Experimental work is always a demanding task and the choice of experiments should always be carefully selected. By using a reduced experimental design several advantages were obtained:

- A study of the effects of varying the feed concentrations were enabled using significantly fewer experiments compared to the conventional approach often encountered in the literature.
- By performing and analysing the transients between the steady state points, a kind of reduced design using step response methodology is automatically obtained. (In this case, due to practical limitations, only steps in H_2, O_2 and NO concentrations were possible.) 13 out of 48 possible combinations were obtained. This efficiently spans the parameter space as pointed out by, e.g. [41] and should thus improve the fitting.
- By applying mainly step changes in two feed components and analyzing both the MLR and kinetic models, the analysis becomes somewhat more complex but substantially more enlightening.

7. Conclusions

A kinetic model for the selective catalytic reduction of NO_x with octane over a $Ag–Al_2O_3$ catalyst has been developed. A key feature of the model is the formation of stable surface nitrate poisons that can be reduced in the presence of hydrogen. The model generally well reproduces the changes due to variations in feed concentrations especially poisoning effects of higher NO concentration and the strong promotion of hydrogen on NO_x reduction. The model also accounts for experimentally observed large temperature increases due to hydrogen oxidation which is an additional side effect of hydrogen feed often neglected in the literature.

Although the model only includes a single role for hydrogen in the reaction mechanism, it should be noted that some of the secondary effects of hydrogen removing nitrate poisons in the model also coincide with other proposed effects of hydrogen in the literature. These include the activation of oxygen [15] or the hydrocarbon reductant [19] and observations that hydrogen results in an increase in the number and variety of adsorbed surface species during the reaction [26].

Acknowledgements

This work was financially supported by the Swedish Science Council, MISTRA (The Foundation for Strategic Environmental Research) and the Swedish Road Administration. It was performed as part of the E4-MISTRA programme (Energy Efficient Reduction of Exhaust Emissions from Vehicles), within the Competence Centre for Catalysis (KCK). KCK is financially supported by Chalmers University of Technology, the Swedish Energy Agency and the member companies: AB Volvo, Volvo Car Corporation, Scania CV AB, GM Powertrain Sweden AB, Haldor Topsoe A/S and The Swedish Space Agency. Financial support from Knut and Alice Wallenberg Foundation, Dnr KAW 2005.0055, is also gratefully acknowledged.

References

[1] T. Miyadera, Applied Catalysis B: Environmental 2 (1993) 199–205.
[2] K. Shimizu, A. Satsuma, T. Hattori, Applied Catalysis B: Environmental 25 (2000) 239–247.
[3] K. Eranen, L.E. Lindfors, F. Klingstedt, D.Y. Murzin, Journal of Catalysis 219 (2003) 25–40.
[4] F. Klingstedt, K. Eranen, L.E. Lindfors, S. Andersson, L. Cider, C. Landberg, E. Jobson, L. Eriksson, T. Ilkenhans, D. Webster, Topics in Catalysis 30–31 (2004) 27–30.
[5] S. Satokawa, J. Shibata, K. Shimizu, A. Satsuma, T. Hattori, Applied Catalysis B: Environmental 42 (2003) 179–186.
[6] R. Burch, J.P. Breen, C.J. Hill, B. Krutzsch, B. Konrad, E. Jobson, L. Cider, K. Eranen, F. Klingstedt, L.E. Lindfors, Topics in Catalysis 30–31 (2004) 19–25.
[7] M. Richter, U. Bentrup, R. Eckelt, M. Schneider, M.M. Pohl, R. Fricke, Applied Catalysis B: Environmental 51 (2004) 261–274.
[8] K. Arve, H. Backman, F. Klingstedt, K. Eranen, D.Y. Murzin, Applied Catalysis A: General 303 (2006) 96–102.
[9] H. Backman, K. Arve, F. Klingstedt, D.Y. Murzin, Applied Catalysis A: General 304 (2006) 86–92.
[10] U. Bentrup, M. Richter, R. Fricke, Applied Catalysis B: Environmental 55 (2005) 213–220.
[11] J.P. Breen, R. Burch, C. Hardacre, C.J. Hill, Journal of Physical Chemistry B 109 (2005) 4805–4807.
[12] P. Sazama, L. Capek, H. Drobna, Z. Sobalik, J. Dedecek, K. Arve, B. Wichterlova, Journal of Catalysis 232 (2005) 302–317.
[13] J. Shibata, K. Shimizu, Y. Takada, A. Shichia, H. Yoshida, S. Satokawa, A. Satsuma, T. Hattori, Journal of Catalysis 227 (2004) 367–374.
[14] J. Shibata, Y. Takada, A. Shichi, S. Satokawa, A. Satsuma, T. Hattori, Journal of Catalysis 222 (2004) 368–376.
[15] K. Shimizu, J. Shibata, A. Satsuma, Journal of Catalysis 239 (2006) 402–409.
[16] K. Shimizu, M. Tsuzuki, K. Kato, S. Yokota, K. Okumura, A. Satsuma, Journal of Physical Chemistry C 111 (2007) 950–959.
[17] B. Wichterlova, P. Sazama, J.P. Breen, R. Burch, C.J. Hill, L. Capek, Z. Sobalik, Journal of Catalysis 235 (2005) 195–200.
[18] A. Satsuma, J. Shibata, K. Shimizu, T. Hattori, Catalysis Surveys from Asia 9 (2005) 75–85.
[19] J. Shibata, K. Shimizu, S. Satokawa, A. Satsuma, T. Hattori, Physical Chemistry Chemical Physics 5 (2003) 2154–2160.
[20] E. Seker, J. Cavataio, E. Gulari, P. Lorpongpaiboon, S. Osuwan, Applied Catalysis A: General 183 (1999) 121–134.
[21] H. Kannisto, H.H. Ingelsten, M. Skoglundh, Journal of Molecular Catalysis A: Chemical (2008), doi:10.1016/j.molcata.2008.12.0003.
[22] J. Dawody, M. Skoglundh, S. Wall, E. Fridell, Journal of Molecular Catalysis A: Chemical 225 (2005) 259–269.
[23] M. Skoglundh, H. Johansson, L. Lowendahl, K. Jansson, L. Dahl, B. Hirschauer, Applied Catalysis B: Environmental 7 (1996) 299–319.
[24] E. Tronconi, P. Forzatti, AIChE Journal 38 (1992) 201–210.
[25] J. Sjöblom, D. Creaser, Computers and Chemical Engineering 31 (2007) 307–317.
[26] J.P. Breen, R. Burch, Topics in Catalysis 39 (2006) 53–58.
[27] J.P. Breen, R. Burch, C. Hardacre, C.J. Hill, Journal of Catalysis 246 (2007) 1–9.
[28] K. Shimizu, J. Shibata, H. Yoshida, A. Satsuma, T. Hattori, Applied Catalysis B: Environmental 30 (2001) 151–162.
[29] M. Yamaguchi, I. Goto, Z.M. Wang, M. Kumagai, Studies in Surface Science and Catalysis 121 (1999) 371–374.
[30] R. Burch, Catalysis Reviews 46 (2004) 271–334.

[31] K. Arve, F. Klingstedt, K. Eränen, J. Wärnå, L.-E. Lindfors, D.Yu. Murzin, Chemical Engineering Journal 107 (2005) 215–220.
[32] T. Furusawa, K. Seshan, J.A. Lercher, L. Lefferts, K. Aika, Applied Catalysis B: Environmental 37 (2002) 205–216.
[33] J.A. Dumesic, D.F. Rudd, L.M. Aparicio, J.E. Rekoske, A.A. Treviño, The Microkinetics of Heterogeneous Catalysis, ACS, Washington, DC, 1993, pp. 26–40.
[34] J.R. Anderson, Structure of Metallic Catalysts, Academic Press, London, 1975, p. 296.
[35] G.W. Busser, O. Hinrichsen, M. Muhler, Catalysis Letters 79 (2002) 49–54.
[36] R. Burch, J.P. Breen, F.C. Meunier, Applied Catalysis B: Environmental 39 (2002) 283–303.
[37] S. Satokawa, Chemistry Letters (2000) 294–295.
[38] K.A. Bethke, H.H. Kung, Journal of Catalysis 172 (1997) 93–102.
[39] F.C. Meunier, J.P. Breen, V. Zuzaniuk, M. Olsson, J.R.H. Ross, Journal of Catalysis 187 (1999) 493–505.
[40] J.H. Lee, S.J. Schmieg, S.H. Oh, Applied Catalysis A: General 342 (2008) 78–86.
[41] J. Sjöblom, D. Creaser, Computers and Chemical Engineering 32 (2008) 3121–3129.